Journal of Medicinal Chemistry

Article

pubs.acs.org/jmc

Discovery and Optimization of a Novel Series of Dyrk1B Kinase Inhibitors To Explore a MEK Resistance Hypothesis

Jason G. Kettle,* Peter Ballard, Catherine Bardelle, Mark Cockerill,† Nicola Colclough, Susan E. Critchlow, Judit Debreczeni, Gary Fairley, Shaun Fillery, Mark A. Graham, Louise Goodwin, Sylvie Guichard, Kevin Hudson, Richard A. Ward, and David Whittaker

Oncology iMed, AstraZeneca, Alderley Park, Macclesfield, SK10 4TG, United Kingdom

Supporting Information

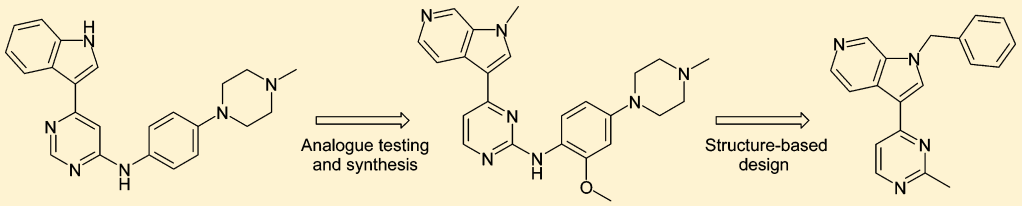

ABSTRACT: Potent and selective inhibitors of Dyrk1B kinase were developed to explore the hypothesis, based on siRNA studies, that Dyrk1B may be a resistance mechanism in cells undergoing a stress response.

INTRODUCTION

Dyrk1B (also known as Mirk or Minibrain-related kinase) is a dual-specificity serine−threonine kinase that has been shown to mediate survival and differentiation in skeletal muscle, in which it is expressed at higher levels relative to that in other normal tissues.[1] It is a member of the Minibrain/Dyrk family of protein kinases that includes Dyrk1A, Dyrk1C, Dyrk2, Dyrk3, Dyrk4A, and Dyrk4B, and, unusually, this family retains the ability to autophosphorylate at a conserved tyrosine residue on the activation loop.[2] Dyrk1B is expressed in several different tumor types and appears to play a key role in maintaining cells in quiescence.[3] Amplification of Dyrk1B expression has been observed in a large subset of ovarian cancers when compared to normal tissue, and depletion of Dyrk1B levels sensitizes these lines to cisplatin treatment, possibly through elevated reactive oxygen species content.[4] Dyrk1B was also found to be highly expressed in osteosarcoma cell lines, and shRNA-mediated target knockdown led to a decrease in proliferation and induction of apoptosis across a range of tumor lines. Osteosarcoma tumors display high metastatic potential, and the relative level of Dyrk1B expression has been correlated with poor outcome in such patients.[5] Additionally, a recent study has implicated a mutation in Dyrk1B kinase with increased adipogenesis and glucose homeostasis in an inherited form of metabolic syndrome.[6] Inhibition of Dyrk1A, by contrast, has been investigated as a strategy for therapeutic intervention in Down's syndrome,[7] where overexpression of the Dyrk1A gene on chromosome 21 has been linked to the impaired neuronal development associated with this genetic disorder through studies in rodents.[8]

Our interest in this kinase was linked to the observation that Dyrk1B is regulated by the kinase Erk and that inhibition of this pathway under serum-free conditions by treatment with a MEK inhibitor caused upregulation of Dyrk1B by 18−20-fold.[1a] In-house studies confirmed upregulation of Dyrk1B mRNA and protein levels when cells are treated with MEK inhibitors, consistent with the hypothesis that Dyrk1B may be a resistance mechanism in cells undergoing a stress response. After knockdown of Dyrk1B, A375 cells were treated with MEK inhibitors AZD6244[9] or AZD8330[10] for 48 h. Total levels of Dyrk1B protein were analyzed by western blot (Figure 1), showing that MEK inhibition causes significant upregulation of Dyrk1B and that this is reduced by prior treatment with siRNA to Dyrk1B. Approximately 60% knockdown of Dyrk1B protein was observed in these experiments. The resulting viability of cells was also evaluated, and it can be seen that treatment of A375 cells with either Dyrk1B siRNA or MEK inhibitor independently results in no appreciable effects on viability; however, the combination of the two results in a significant enhancement of cell death (Figure 2).

Despite this interesting biology, there remains a lack of highly potent and selective tool molecules with which to elucidate the role of Dyrk family kinases in a disease setting, particularly with regard to recapitulation of siRNA knockdown studies, and also ultimately as *in vivo* probes.[11] The beta-carboline alkaloid harmine **1** (Figure 3) has been most studied in the context of Dyrk1A inhibition in a neuritogenesis setting, although this tool compound may be more accurately described as a mixed Dyrk1A and 1B inhibitor, with reported enzyme IC_{50}'s of 33 and 166 nM, respectively. It has much lower potency against Dyrk2 (2 μM) and Dyrk4 (74 μM).[12] Despite

Received: January 19, 2015

DOI: 10.1021/acs.jmedchem.5b00098
J. Med. Chem. XXXX, XXX, XXX−XXX

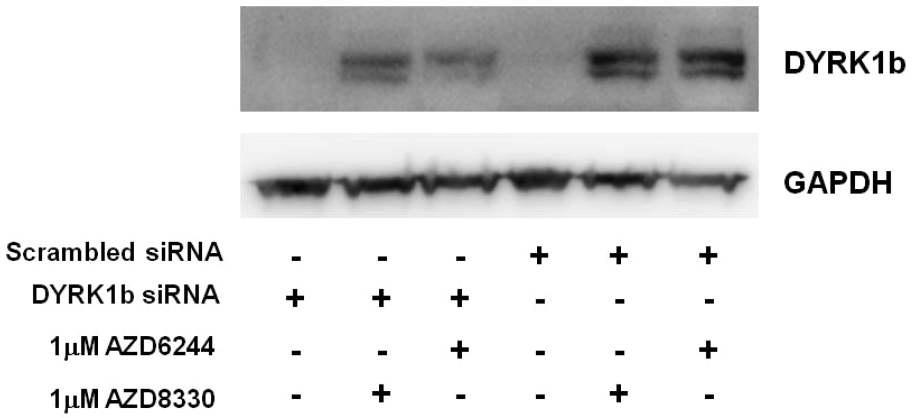

Figure 1. MEK inhibitor treatment of A375 melanoma cells results in significant upregulation of Dyrk1b, which is reduced by siRNA targeting Dyrk1b. Western blot is representative of at least two separate experiments.

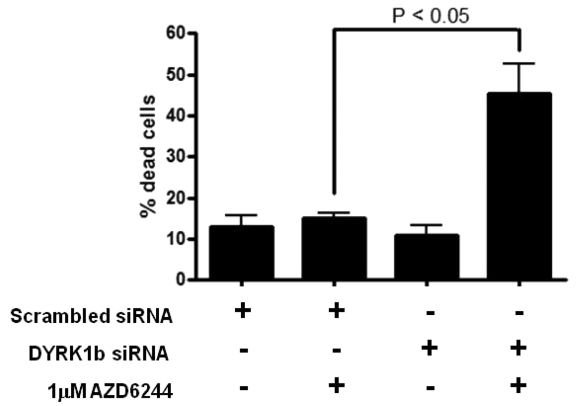

Figure 2. siRNA-mediated knockdown of DYRK1b increases cell death in AZD6244-treated A375 cells. The percentage of dead cells plotted is the mean and SEM from four separate experiments. Statistically significant differences, compared with control (scrambled) siRNA, are indicated.

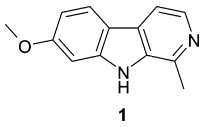

1

Figure 3. Literature reported inhibitor of Dyrk1A and Dyrk1B, harmine.

its generally good selectivity across other kinases,[13] the utility of harmine as a probe compound, particularly *in vivo*, may be limited by other off-target pharmacologies, which include cytotoxicity,[14] PPARgamma induction,[15] and potent inhibition of monoamine oxidase A.[16] Herein, we report our studies aimed at generating potent and selective small molecule inhibitors of the Dyrk family enzymes, in particular Dyrk1B, for use as *in vivo* probes to further delineate the role of these targets in disease.

CHEMISTRY

Azaindole **2** was brominated at C-3 to give compound **3**, which was subsequently protected to give benzenesulfonyl azaindole **4** (Scheme 1). Boronate ester **5** served as the key intermediate for all anilinopyrimidine inhibitors and was derived from **4** via coupling with bis(pinacolato)diboron. Capping of **5** with a sulfonyl group was required to ensure efficient coupling in the subsequent step, which, in the case of 2,4-dichloropyrimidine, occurred selectively at C-4 to give pyrimidine **6**. *N*-Methyl azaindole analogues were prepared from **6** in a sequence involving deprotection to give **7** and methylation to give chloropyrimidine **8**. Introduction of the 2-anilino moiety was realized under mild acid catalysis to give **19**. Styrene analogue **31** was obtained directly from **6** via Suzuki cross-coupling and deprotection of the azaindole *in situ*. A modified route was adopted for synthesis of 2-methylpyrimidine analogues **32** and **33** (Scheme 2). Here, azaindole **2** was first acetylated to give **3**. Protection of the azaindole nitrogen to give **10** was followed by a short sequence to build up the pyrimidine ring directly. Reaction of **10** with DMF acetal to give **11** was followed by condensation with acetimidamide and resultant loss of the protecting group to yield 2-methylpyrimidine **32**. Alkylation of the azaindole nitrogen of **32** was achieved under Mitsunobu conditions to give benzyl analogue **33**.

6-AZAINDOLE ANILINOPYRIMIDINES AS INHIBITORS OF DYRK1B

Kinases Dyrk1A, Dyrk2, and Dyrk3 were available to us for screening through our collaboration with the MRC Protein Phosphorylation Unit at the University of Dundee together with a range of other serine−threonine kinases. This panel of enzymes was utilized by discovery projects to assess broader kinase selectivity as part of the lead optimization process. Consequently, there existed a significant amount of data against these isoforms for current and past project compounds. Compound **18**, initially synthesized as part of an internal program to target IGF, had been profiled in this panel and showed significant inhibition at 1 μM (90, 92, and 83% inhibition of Dyrk1A, 2, and 3, respectively), albeit with only a moderately selective profile. Of the 71 kinases tested in this panel, **18** showed >75% inhibition against 11 kinases (and >50% inhibition against 27/71). Internal testing confirmed **18** to be a highly potent inhibitor of Dyrk1B with an IC_{50} of 4 nM. This initial lead compound was followed up with screening of further analogues, with the aim of improving the Dyrk1B potency and overall kinase selectivity and delivering tool molecules suitable for exploring the role of Dyrk1B inhibition *in vivo*.

Compound **12** (Table 1), based on a 4,6-pyrimidine scaffold and an undecorated indole at C-4, has modest enzyme potency but weak activity in cells, with reasonable (28-fold) selectivity over IGF. Selectivity over cell cycle kinase CDK2 was also

DOI: 10.1021/acs.jmedchem.5b00098
J. Med. Chem. XXXX, XXX, XXX−XXX

Scheme 1. Synthesis of Key 6-Azaindole Intermediates and Inhibitors 19 and 31[a]

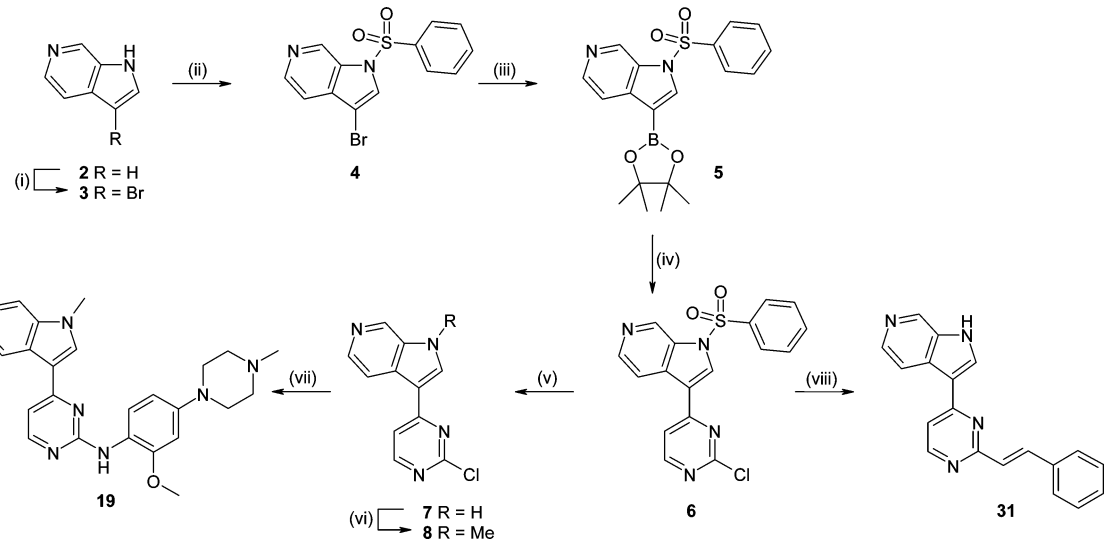

[a]Reagents and conditions: (i) Br_2, $NaHCO_3$, MeOH, 0 °C, 3 h; (ii) $PhSO_2Cl$, aq. NaOH, TBAHS, DCM, 0 °C, 1 h; (iii) PdCl2(dppf), Bis(pinacolato)diboron, KOAc, DME, 80 °C, 18 h; (iv) $Pd(PPh_3)_4$, 2,4-dichloropyrimidine, aq. Na_2CO_3, dioxane, 80 °C, 1 h; (v) aq. Na_2CO_3, dioxane, 120 °C, 0.5 h; (vi) NaH, MeI, 0 °C, 2 h; (vii) *p*TSA, 2-methoxy-4-(4-methylpiperazin-1-yl)aniline, NMP, 200 °C, 2 h; (viii) $PdCl_2(PPh_3)_2$, *trans*-stilbeneboronic acid, $K_2PO_4{\cdot}H_20$, 130 °C, 0.5 h, then aq. Na_2CO_3, 140 °C, 40 min.

Scheme 2. Synthesis of Diverse Dyrk1B Inhibitors 32 and 33[a]

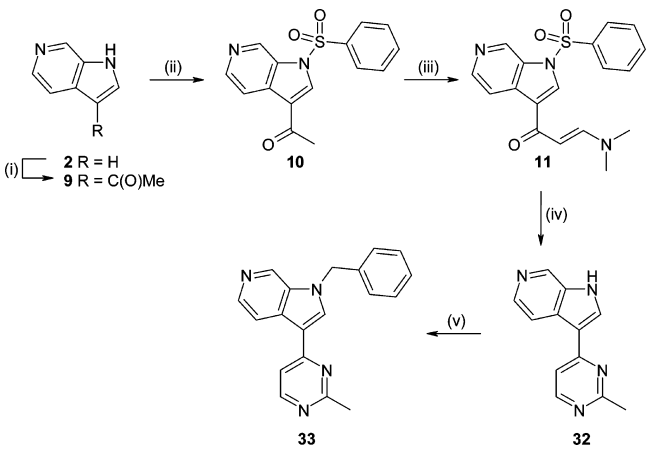

[a]Reagents and conditions: (i) AcCl, $AlCl_3$, 25 °C, 18 h; (ii) $PhSO_2Cl$, aq. NaOH, TBAHS, DCM, 0 °C, 40 min; (iii) 1,1-di-*tert*-butoxy-*N*,*N*-dimethylmethanamine, DMF, 80 °C, 1 h; (iv) acetimidamide·HCl, KO-*t*-Bu, DMA, 150 °C, 1 h; (v) $PhCH_2OH$, DIAD, PPh_3, THF, 25 °C, 18 h.

routinely assessed since compounds from this chemotype had provided the original leads for exploitation in IGF,[17] and **12** showed good selectivity over CDK2. Introduction of a 6-aza substituent to the indole as in **13**, however, has a dramatic effect on Dyrk1B potency, increasing 40-fold to 2 nM, and is suggestive of a specific interaction within the kinase active site. This change also appears to be highly unfavorable in IGF: the compound is inactive up to 100 μM, although selectivity against CDK2 is slightly reduced. Comparison of the *in vivo* clearances of these two compounds indicates exceptionally high clearance for the aza-analogue, which is not explained from *in vitro* clearance values, suggestive of an extrahepatic component to clearance. Introduction of an ortho-methoxy group at the hinge aniline, as in **14**, maintains Dyrk1B potency and improves selectivity over CDK2. The impact of an ortho-substituent in diminishing CDK2 potency has been documented,[18] and because such a strategy had previously been employed by us to gain CDK2 selectivity in the IGF targeting series, it is unsurprising to see measurable, albeit weak, IGF inhibition for this change. *In vivo* clearance for this compound again remains above liver blood flow, however. The much increased enzyme potency for **13** and **14** results in submicromolar cellular activity for these agents. Conversion of the basic side chain in **14** to a neutral, acetoxy-capped piperazine, as in **15**, was investigated because the transition from a basic to a neutral chemotype in optimization of the IGF series was commensurate with significantly improved DMPK. In the case of **15**, unfortunately, *in vivo* clearance remained stubbornly high and was coupled with a slight attenuation of Dyrk1B potency. Methylation of **15** to give **16** was undertaken in an effort to understand the role, if any, of the azaindole NH on clearance. Gratifyingly, *in vivo* clearance was observed to drop significantly to a more acceptable 16 mL/min/kg for this compound, with a slight drop in potency relative to that of **15** (2-fold). However, when dosed orally, **16** exhibited a low bioavailability of 5%, consistent with poor absorption. Transformation of 4,6-pyrimidine **15** to the matched 2,4-pyrimidine **17** highlights the role the hinge binding group plays in both potency and selectivity. Dyrk1B inhibition is similar for both scaffolds, but this compound, as expected, shows much greater activity versus IGF and CDK2. The *in vivo* clearance of **17** appears lower compared to that of **15**, although it is still in excess of liver blood flow. Finally, reversion of the side chain back to a basic piperazine, as in **18**, gives a highly potent Dyrk1B inhibitor with potent inhibition in cells, with an IC_{50} of 85 nM. IGF and CDK2 appear to be largely indifferent to this change, resulting in an improved selectivity margin for **18**. Compound **18** is the pyrimidine matched pair to **14**; this switch to a 2,4-pyrimidine again confirms the largely similar Dyrk1B profile but with attenuated selectivity versus IGF and CDK2.

This initial exploration highlighted the azaindole moiety as the likely cause of the high observed *in vivo* clearance,

DOI: 10.1021/acs.jmedchem.5b00098
J. Med. Chem. XXXX, XXX, XXX−XXX

Table 1. Profile of Anilinopyrimidine Inhibitors of Dyrk1B

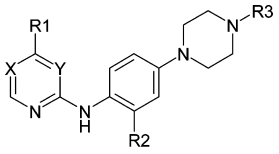

A 4,6-Pyrimidine X=N, Y=CH
B 2,4-Pyrimidine X=CH, Y=N

					IC$_{50}$ (μM)				Rat DMPK		
ID	Core	R1	R2	R3	Dyrk1B[a]	Cell[a,b]	IGF[a]	CDK2[a]	Cl$_{int}$[c]	Cl[d]	F%[e]
12	A		H	Me	0.085	9.965	2.409	33.215	49	42[f]	13
13	A		H	Me	0.002	0.453	>100	0.577	13	1790	
14	A		MeO	Me	0.001	0.282	34.125	12.295	11	375	
15	A		MeO	Ac	0.016		40.515	14.060	9	239	
16	A		MeO	Ac	0.034		>100	14.789	11	16	5
17	B		MeO	Ac	0.009		0.965	1.995	< 1	137	
18	B		MeO	Me	0.004	0.085	1.489	1.819	21		

[a]All IC$_{50}$ data are reported as micromolar and are the mean of at least $n = 2$ independent measurements. Each has a SEM ± 0.2 log units. [b]Inhibition of phosphorylation of Dyrk pS421 of transiently overexpressed cMyc-Dyrk in Cos-1 cells following a 5 h treatment with compound. [c]Cl$_{int}$ (μL/min/1 × 10^6 cells) in Wistar Han rat hepatocytes. [d]Plasma Cl (mL/min/kg) in Wistar Han rats dosed at 2 μmol/kg. [e]Bioavailability of an oral solution in Wistar Han rats dosed at 3 μmol/kg. [f]Blood Cl.

particularly in light of the lowered clearance with indole **12** and methylated azaindole **16**. As it appeared that both an azaindole and basic side chain are required for high potency, we further examined the role of substitution on the heterocycle to modulate metabolism (Table 2). *N*-Methyl azaindole **19**, the basic analogue of **16**, is a potent inhibitor of Dyrk1B kinase with good selectivity over IGF and CDK2. As with **16**, this compound showed low *in vitro* and *in vivo* clearance in rat and, gratifyingly, an improved, yet modest, bioavailability of 22%. It is tempting to speculate that the reduced bioavailability seen with neutral **16** is as a consequence of its much reduced aqueous solubility (pH 7.4) relative to that of **19** (53 versus >755 μM, respectively). Methylation adjacent to the aza-nitrogen at C5 to give **20**, or C7 to give **21**, gave compounds with very low turnover in rat hepatocytes, although in both of these compounds, potent IGF inhibition was observed. Consistent with earlier compounds, and despite low clearance *in vivo* for **21**, no oral exposure was seen for this compound where the azaindole nitrogen was not methylated. Combining the features of **19** and **21** to give dimethylated azaindole **22** gave a low clearance compound with the selectivity profile somewhat restored, although bioavailability was lower at 14%, again possibly a consequence of lower solubility (4 μM).

DOI: 10.1021/acs.jmedchem.5b00098
J. Med. Chem. XXXX, XXX, XXX−XXX

Table 2. Profile of Methylated Azaindole Inhibitors of Dyrk1B

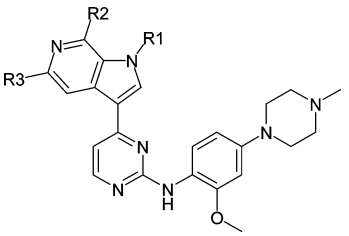

				IC_{50} (μM)				Rat DMPK		
ID	R1	R2	R3	Dyrk1B[a]	Cell[a,b]	IGF[a]	CDK2[a]	Cl_{int}[c]	Cl[d]	F%[e]
19	Me	H	H	0.003	0.042	0.779	4.473	18	27	22
20	H	H	Me	0.004		0.072	10.476	6		
21	H	Me	H	0.005	0.083	0.051	17.368	<5	38	0
22	Me	Me	H	0.009	0.168	3.174	13.713	6	24	14

[a]All IC_{50} data are reported as micromolar and are the mean of at least $n = 2$ independent measurements. Each has a SEM ± 0.2 log units. [b]Inhibition of phosphorylation of Dyrk pS421 of transiently overexpressed cMyc-Dyrk in Cos-1 cells following a 5 h treatment with compound. [c]Cl_{int} (μL/min/1×10^6 cells) in Wistar Han rat hepatocytes. [d]Plasma Cl (mL/min/kg) in Wistar Han rats dosed at 2 μmol/kg. [e]Bioavailability of an oral solution in Wistar Han rats dosed at 3 μmol/kg.

STRUCTURAL BASIS FOR POTENCY AND SELECTIVITY

Insights into the binding mode of the series benefited from the solved kinase crystal structures of closely related compound **23** in both TTK and IGF1R (Figures 4 and 5), which had been

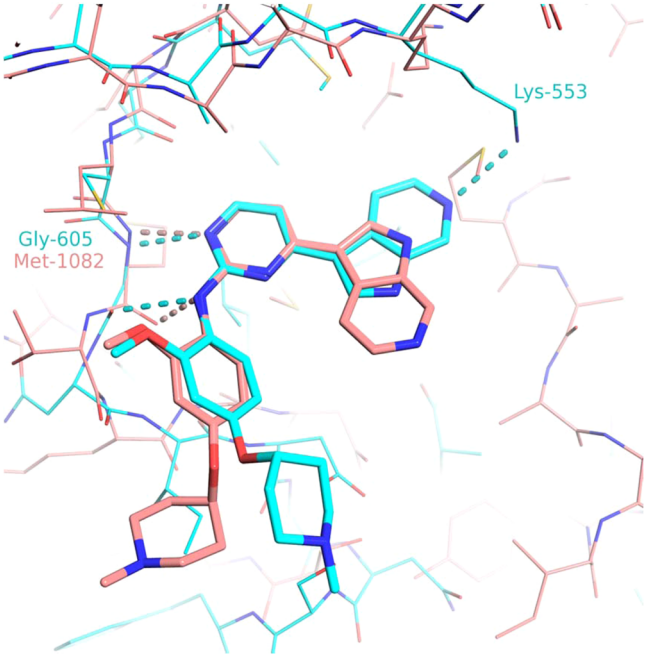

Figure 4. Crystal structures of compound **23** bound in IGF1R (pink) and TTK (cyan) showing the change in orientation of the C-4 azaindole headgroup.

solved in-house previously (PDB codes 4D2S and 4D2R, respectively). This compound exhibited an IC_{50} of 0.02 μM against TTK and 3.3 μM against IGF1R in biochemical assays, allowing these systems to act as potential structural surrogates. The Dyrk1B potency of this compound was 0.14 μM. The template binds in a traditional anilino-pyrimidine binding mode with a hydrogen-bond acceptor−donor pair interaction with the hinge region of each kinase, Gly-605 in TTK and Met-1082 in

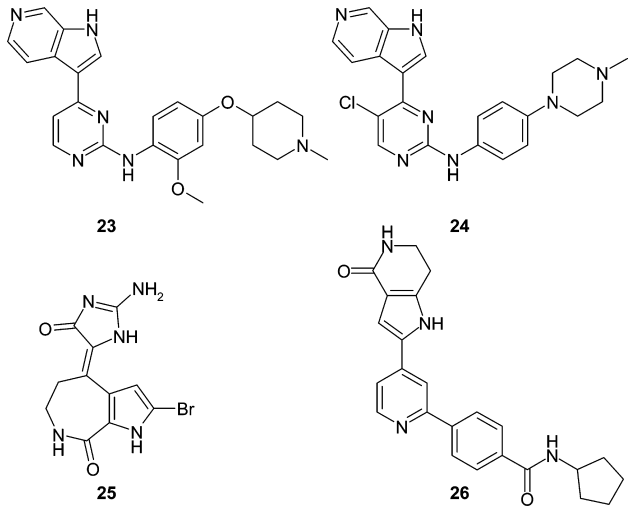

Figure 5. Compounds used to infer the binding mode of azaindoles in Dyrk1B.

IGF1R. The basic piperidine side chain on the anilino group is directed into the solvent channel, as is commonly observed in kinase inhibitor bound crystal structures. Interactions in this region can impact inhibitor potency and selectivity but most notably allow for modulation of physical properties. Interestingly, there appear to be differences in the binding mode conformation of the 6-azaindole group between the two structures. The IGF1R structure shows the 6-azaindole group directed back toward the solvent-exposed region of the pocket; the azaindole itself does not appear to make any specific interactions to explain the role of the nitrogen on the azaindole ring. Conversely, in the TTK structure, this group is directed toward the selectivity pocket region and the aza-nitrogen appears to make a specific interaction with the conserved lysine residue (Lys-553) that is present in most kinases. It is perhaps nonintuitive that making a specific interaction with this lysine residue would lead to improved selectivity; it is, however, likely that the environment around the lysine is variable across the kinome, and the ability of the azaindole group to bind may vary between different kinases. The increased potency of compound **23** in TTK (and selectivity versus IGF1R) may initially suggest

DOI: 10.1021/acs.jmedchem.5b00098
J. Med. Chem. XXXX, XXX, XXX−XXX

this binding mode is also the preferred one in Dyrk1B. However, we additionally observed that introduction of a 5-chloro group to the pyrimidine template, as in compound **24**, maintains potency in Dyrk1B (IC_{50} of 0.025 μM) but shows much reduced selectivity (with IC_{50}'s of 0.02 μM in CDK2 and 0.03 μM in IGF1R). The addition of this chlorine would be expected to cause a steric clash with the 6-azaindole and enforce a binding mode similar to the IGF1R structure, explaining the lowered selectivity. The presence of the chlorine itself may also increase the potency of compound **24** against other kinases directly, especially kinases with lipophilic gatekeeper residues such as methionine, which is the gatekeeper of IGF1R, the original target of this series. That Dyrk1B potency is maintained with both a 5-H and 5-Cl pyrimidine may support a hypothesis that the preferred Dyrk1B binding mode to gain selectivity is as observed in TTK, but that the alternative, IGF1R-like, binding mode is also tolerated in Dyrk1B if additional substituents prohibit access to the more selective TTK orientation.

To further develop our understanding of the binding modes of these compounds, a number of kinases were identified that had homologous kinase domain sequences. At the time this work was undertaken, there were no published Dyrk family crystal structures available; therefore, of most interest were kinases that were likely to share structural similarity to Dyrk1B in the ATP pocket. The published CLK1 structure bound with 10z-hymenialdisine **25** (PDB code 1Z57; Figure 6) appeared to

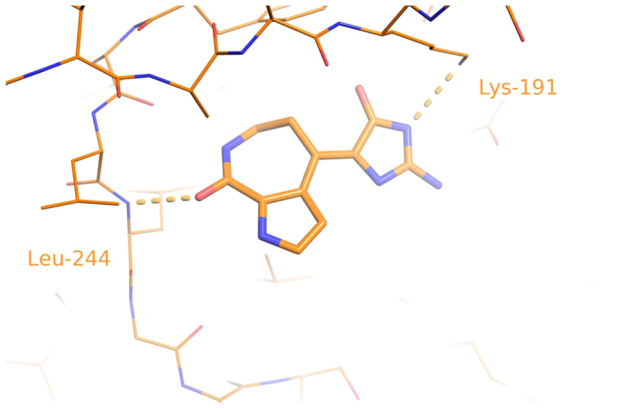

Figure 6. Structure of 10z-hymenialdisine **25** bound to CLK1.

provide a suitable structural surrogate with ~92% sequence homology to Dyrk1B in the ATP pocket, although the overall sequence homology was only ~31%. Interestingly, the aminoimidazolone group of **25** directly interacts with the conserved lysine (Lys-191), as is similarly observed for the 6-azaindole group of compound **23** in the TTK structure. Additionally, the carbonyl group of Leu-244 on the hinge is observed with a pronounced twist, resulting in this group being less accessible to an inhibitor relative to that which is commonly observed across kinases. The equivalent carbonyl group was shown to form a direct hydrogen bond with the C-2 anilino group of **23** in both the IGF1R and TTK structures, but this interaction appeared unlikely to be optimal if this more signficant twist was observed in Dyrk1B. In addition, the sequence overlay of CLK1 with Dyrk1B highlights a leucine residue in Dyrk1B in the same position as Leu-244 of CLK1. We therefore speculated that Dyrk1B may accommodate a greater variety of functionality in this position, more specifically agents lacking a donor in the established 1,3-donor−acceptor hinge interaction.

Wider testing of kinase templates from our screening collection that lacked the hydrogen-bond donor in this position identified a published MK2 inhibitor, **26**,[19] which, in our hands, had an IC_{50} 0.043 μM in Dyrk1B. A crystal structure (PDB code 2P3G) of a compound from this series bound in MK2 confirms interaction with the hinge region via the pyridine, with the C-2 phenyl ring passing close to the hinge region and directed toward solvent. It is also interesting to note that this molecule appears to interact with the conserved lysine (Lys-93) of MK2 (and therefore most likely Dyrk1B also) in a similar fashion as that of compound **23** in TTK through the amide of the C-4 group. Subsequent to this work, crystal structures of Dyrk1A have been released into the public domain, and one example is bound with harmine **1** (PDB code 3ANR; Figure 7).

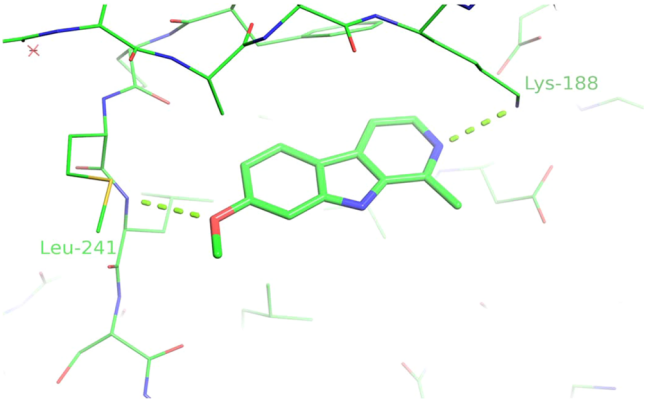

Figure 7. Crystal structure of harmine **1** bound to Dyrk1A.

This structure shows the inhibitor interacting with the salt bridge (Lys-188) via the pyridine group, again reminiscent of the interaction of the 6-azaindole with this group in the TTK structure, and provides further evidence to support the proposed binding mode of this series in Dyrk1B. Harmine appears to interact with the hinge region via a hydrogen-bond acceptor from the methoxy group to the backbone of Leu-241. Gratifyingly, this structure also demonstrates the twist of the carbonyl in the hinge region that we had predicted and suggests that such a feature is likely to be observed in Dyrk1B also. Reviewing the psi angle from the carbonyl across the kinase structures described, IGF1R showed $\psi = -92.6°$, TTK, $\psi = -17.2°$, CLK1, $\psi = 0.2°$, and Dyrk1A, $\psi = 6.7°$. This highlights the most significant twist was observed in the CLK1 and Dyrk1A structures, although the TTK structure also showed the carbonyl to be out-of-plane relative to IGF1R (Figure 8).

Such subtle differences in hinge region conformation appear to allow selectivity to be achieved across certain kinases. A more significant conformational change in the hinge region has been reported in P38α, where a flip of the hinge region residues Leu-108 and Met-109, which changes the interaction pattern of the hinge, led to the identification of inhibitors with increase selectivity.[20]

A HYBRID 2-PHENYLPYRIMIDINE SERIES

Hybridization of the favored Dyrk1B azaindole pharmacophore with reported MK2 inhibitor **26**, in a manner that places a direct phenyl group linked to the C-2 position of the pyrimidine hinge binder, gave **27**. As hypothesized, deletion

DOI: 10.1021/acs.jmedchem.5b00098
J. Med. Chem. XXXX, XXX, XXX−XXX

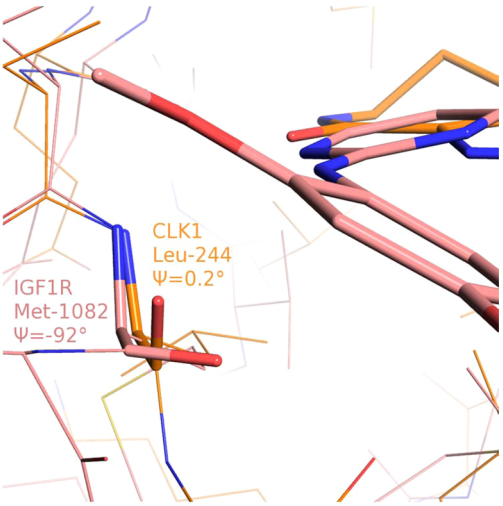

Figure 8. Structure of 10z-hymenialdisine **25** bound to CLK1 (orange) overlaid with compound **23** bound in IGF1R (pink). The atoms used in the measurement of the psi torsion are indicated in bold.

of the hinge hydrogen-bond donor was tolerated and led to potent inhibition of Dyrk1B (Table 3). Selectivity against IGF and CDK2 was also improved, and it was anticipated that wider kinase selectivity would also be enhanced. Further optimization of **27** was undertaken, with an emphasis on reducing lipophilicity. Replacement of the terminal amide of **27** with a methanesulfonyl moiety gave **28**, which showed modest cellular activity but with excellent selectivity. Despite this, *in vitro* clearance was high in rat hepatocytes. Building upon the SAR for methyl substitution on the azaindole delineated earlier for the anilinopyrimidine series, *N*-Methyl analogue **29** and C7-Methyl analogue **30** were also synthesized. Compound **29** with submicromolar cellular potency and increased selectivity versus IGF and CDK2 benefited from low *in vitro* and *in vivo* turnover and a reasonable bioavailability of 37%. Unlike that in the aniline series, the low solubility of **29** (2 μM) did not preclude good absorption, presumably due to the excellent permeability as measured in Caco2 cells. The C7-Methyl analogue **30** had a similar overall profile, albeit with reduced potency and compromised bioavailability, which is consistent with the *in vivo* profile of this headgroup in compound **21**, the equivalent compound in the aniline series.

Encouraged by the unusual observation that the donor can be dispensed with in the usual donor−acceptor hinge interaction of this anilinopyrimidine series, we sought to further explore the tolerance for functionality in this region. Extending the aromatic group at C-2 out by spacing with a *trans*-alkene gave compound **31** (Table 4), which was a potent inhibitor of Dyrk1B in enzyme and cell assays, with good selectivity versus IGF and CDK2. Compound **32** indicates that substantial activity is retained in this template even when the C-2 group is pared to as small a group as methyl. Inhibitor **32**, with a molecular weight of just 210 Da, represents a highly ligand efficient (LE), almost fragment like, yet potent inhibitor of Dyrk1B enzyme with an IC_{50} of 0.017 μM (LE defined as pIC_{50}/heavy atom count = 0.49). Alkylation of **32** with a benzyl group gave **33**, which recovered a significant amount of the cellular potency lost in compound **32** and illustrates the scope for additional optimization in this region of the binding site. Finally, in exploration of alternative hinge binding motifs, compound **34**, a structurally interesting fusion of 6- and 7-azaindole moieties, also represents a highly potent scaffold for Dyrk1B inhibition. In this case, restoration of the 1,3-donor−acceptor motif leads to increased CDK2 inhibition, however.

SELECTIVITY PROFILES

To assess the broader kinase selectivity of the Dyrk inhibitors, representative compounds were screened in a diverse panel of 124 kinases at a single concentration of 1 μM. Inhibitors **19**, **31**, and **33** were chosen as being a potent, structurally diverse set, representing examples from the anilinopyrimidine and hybrid series, and the kinome profile of these compounds is shown in summary form in Table 5. Complete panel data is available as Supporting Information. Generally, all compounds showed a reasonable selectivity profile. Anilinopyrimidine **19** showed a moderately selective profile, although it was the least selective of the three, with 10% of the panel inhibited >75%. Hybrid **33** appeared to be the most selective of these, with no kinases

Table 3. 2-Phenylpyrimidine Inhibitors of Dyrk1B

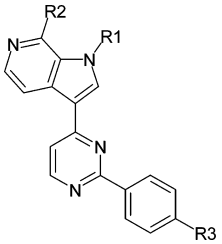

				IC_{50} (μM)				Rat DMPK		
ID	R1	R2	R3	Dyrk1B[a]	Cell[a,b]	IGF[a]	CDK2[a]	Cl_{int}[c]	Cl[d]	F%[e]
27	H	H	C(O)NH-c-Pentyl	0.098		67.727	45.885	32		
28	H	H	SO_2Me	0.021	0.898	>100	16.884	129		0
29	Me	H	SO_2Me	0.012	0.810	>10	>100	8	23	37
30	H	Me	SO_2Me	0.014	2.118	>29	>100	9	24	4

[a]All IC_{50} data are reported as micromolar and are the mean of at least $n = 2$ independent measurements. Each has a SEM ± 0.2 log units. [b]Inhibition of phosphorylation of Dyrk pS421 of transiently overexpressed cMyc-Dyrk in Cos-1 cells following a 5 h treatment with compound. [c]Cl_{int} (μL/min/1×10^6 cells) in Wistar Han rat hepatocytes. [d]Plasma Cl (mL/min/kg) in Wistar Han rats dosed at 2 μmol/kg. [e]Bioavailability of an oral solution in Wistar Han rats dosed at 3 μmol/kg.

DOI: 10.1021/acs.jmedchem.5b00098
J. Med. Chem. XXXX, XXX, XXX−XXX

Table 4. 2-Alkylpyrimidine Inhibitors of Dyrk1B

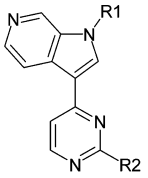

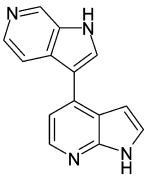

34

			IC$_{50}$ (μM)			
ID	R1	R2	Dyrk1B[a]	Cell[a,b]	IGF[a]	CDK2[a]
31	H	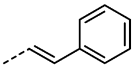	0.007	0.192	46.942	5.176
32	H	Me	0.017	3.069	> 100	38.379
33	Bn	Me	0.007	0.194	> 100	56.703
34			0.003	0.378	7.922	0.314

[a]All IC$_{50}$ data are reported as micromolar and are the mean of at least n = 2 independent measurements. Each has a SEM ± 0.2 log units. [b]Inhibition of phosphorylation of Dyrk pS421 of transiently overexpressed cMyc-Dyrk in Cos-1 cells following a 5 h treatment with compound.

Table 5. Kinase Selectivity Profiles of Representative Dyrk1B Inhibitors

ID	percent kinases inhibited >75%	percent kinases inhibited >50%	kinases most potently inhibited
19	10	16	CaMKIIβ, Flt3, DRAK1
31	6	15	Flt1, Flt3, MLK1
33	0	0	Mnk2, PI3KC2γ, Flt3

inhibited above the 50% level. By comparison, hybrid **31** was slightly less selective, and it is tempting to speculate that an alternative binding modality through the azaindole nitrogen acceptor might be accessible for some of the kinases inhibited by this compound. It was determined that compound **19** was also able to potently inhibit other Dyrk family members, albeit with selectivity in favor of Dyrk1B (IC$_{50}$'s of 3, 30, and 190 nM against Dyrk1B, Dyrk1A, and Dyrk2, respectively).

CELLULAR PROFILING

A primary hypothesis was developed that a Dyrk1B inhibitor in combination with a MEK inhibitor would result in increased cell death in solid tumors, with melanoma being an example of a tumor type where a strong response might be expected. It was observed that tumor cells upregulate Dyrk1B in response to MEK inhibitors and that siRNA to Dyrk1B sensitized multiple tumor cell lines to MEK inhibitors, including induction of cell death in the most sensitive models. A selection of potent, structurally diverse Dyrk1B inhibitors assembled in the course of this study was profiled in A375 melanoma cells in combination with MEK inhibitor AZD6244 (Figure 9). The combination of MEK inhibitor and siRNA leads to an increase in cell death over that with either modality alone. In contrast to this, we observed no effect of structurally diverse and potent Dyrk1B inhibitors **19**, **31**, and **33** in combination with MEK inhibitor in this assay. It is noteworthy that **33**, shown to be a

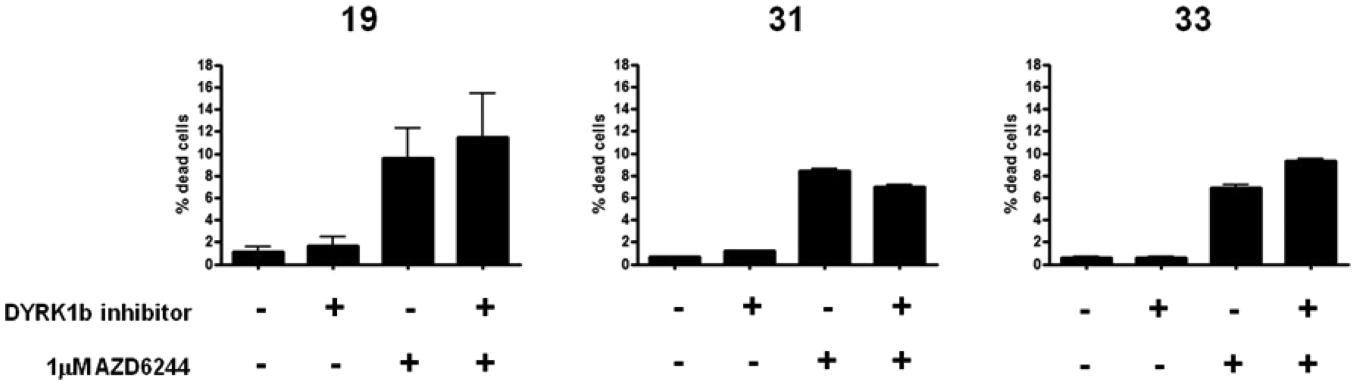

Figure 9. Impact on survival of the combination of MEK inhibitor AZD6244 and Dyrk1B inhibition on A375 melanoma cell line. Dyrk1B inhibition is affected with inhibitors **19**, **31**, and **33**. A375 cells were treated with AZD6244 in the presence or absence of DYRK1b inhibitors **19**, **31**, or **33** at a concentration of 1.33 μM for 72 h. The viability of cells was evaluated using CellTraceTM calcein green AM and propidium iodide (PI) stains. The percentage of dead cells plotted is the mean and SEM from at least two separate experiments.

DOI: 10.1021/acs.jmedchem.5b00098
J. Med. Chem. XXXX, XXX, XXX−XXX

highly selective inhibitor of Dyrk1B, with cellular activity, showed no effect in sensitization. Taken together, we conclude that Dyrk1B kinase inhibition with a small molecule ATP competitive inhibitor does not recapitulate the effects seen in combination with target knockdown through siRNA. That gene silencing through target knockdown leads to a different phenotype from that seen with small molecule inhibition is perhaps not unexpected, since the former may disrupt critical protein complexes or inhibit other functional activities independent of kinase activity.[21] Compound **19** has recently been profiled in depth for its role in inhibiting Dyrk1B in a cellular setting and was shown to potently inhibit Dyrk1B induced phosphorylation of cyclin D1 at T286.[22] Dyrk1B is also known to autophosphorylate at Y273, and, in contrast, this activity is not abolished by either compound **19** or, indeed, harmine **1**. This is one example of a functionally different consequence from that observed with gene knockdown approaches, but it is not possible to attribute with certainty the lack of observed sensitization to MEK inhibition to this specific observation.

CONCLUSIONS

Treatment of a variety of cell lines either with a MEK inhibitor or under conditions of serum starvation leads to significant upregulation of Dyrk1B, and combination of this with silencing of Dyrk1B leads to enhanced cell death. A diverse array of potent, selective, and cellular active Dyrk1B inhibitors has been developed through a combination of targeted screening and structure-based design, but these do not recapitulate the sensitization seen with siRNA. Nevertheless, these compounds may serve as useful tools to further delineate the role of Dyrk1B in cells and may provide useful tools in further exploring the role of the Dyrk family enzymes in an *in vivo* disease model setting.

EXPERIMENTAL SECTION

Chemistry. All reactions were performed under inert conditions (nitrogen) unless otherwise stated. Temperatures are given in degrees celsius (°C); operations were carried out at room or ambient temperature, that is, at a temperature in the range of 18−25 °C. All solvents and reagents were purchased from commercial sources and used without further purification. For coupling reactions, all solvents were dried and degassed prior to reaction. Reactions performed under microwave irradiation utilized either a Biotage Initiator or CEM Discover microwave. Upon work up, organic solvents were typically dried prior to concentration with anhydrous $MgSO_4$ or Na_2SO_4. Flash silica chromatography was typically performed on an Isco Companion, using Silicycle silica gel, 230−400 mesh 40−63 μm cartridges, Grace Resolv silica cartridges or Isolute Flash Si or Si II cartridges. Reverse-phase chromatography was performed using a Waters XBridge Prep C18 OBD column, 5 μ silica, 19 mm diameter, 100 mm length, using decreasingly polar mixtures of either water (containing 1% NH_3) and acetonitrile or water (containing 0.1% formic acid) and acetonitrile as eluents. Analytical LC-MS was performed on a Waters 2790 LC with a 996 PDA and 2000 amu ZQ single quadrupole mass spectrometer using a Phenomenex Gemini 50 × 2.1 mm 5 μm C18 column; UPLC was performed on a Waters Acquity binary solvent manager with Acquity PDA and an SQD mass spectrometer using a 50 × 2.1 mm 1.7 μm BEH column from Waters, and purities were measured by UV absorption at 254 nm or TIC and are ≥95% unless otherwise stated. NMR spectra were recorded on a Bruker Av400 or Bruker DRX400 spectrometer at 400 MHz in DMSO-d_6 at 303 K unless otherwise indicated. ^{1}H NMR spectra are reported as chemical shifts in parts per million (ppm) relative to an internal solvent reference. Yields are given for illustration only and are not necessarily those which can be obtained by diligent process development; preparations were repeated if more material was required.

3-Bromo-1*H*-pyrrolo[2,3-*c*]pyridine (3). A solution of bromine (8.7 mL, 169 mmol) in methanol (300 mL) was added dropwise to a stirred mixture of 1*H*-pyrrolo[2,3-*c*]pyridine **2** (20 g, 169 mmol) and sodium hydrogen carbonate (42.7 g, 508 mmol) in methanol (600 mL) at −5 °C at such a rate that the internal temperature remained below 0 °C. The resulting mixture was allowed to warm to room temperature and stirred for 3 h. The reaction mixture was evaporated to dryness, redissolved in ethyl acetate (1 L), and washed sequentially with water (2 × 1 L) and saturated brine (1 L). The organic layer was dried, filtered, and evaporated to afford crude product. The crude product was purified by recrystallization from toluene (1 L) to afford **3** (17.7 g, 53%) as a beige solid. ^{1}H NMR δ 7.41 (1H, dd), 7.81 (1H, s), 8.21 (1H, d), 8.78 (1H, d), 11.98 (1H, brs); *m*/*z* (ES+) $(M + H)^+$ = 199; HPLC t_R = 1.57 min.

3-Bromo-1-(phenylsulfonyl)-1*H*-pyrrolo[2,3-*c*]pyridine (4). Benzenesulfonyl chloride (13.7 mL, 108 mmol) was added dropwise to compound **3** (17.7 g, 90 mmol), tetrabutylammonium hydrogensulfate (0.9 g, 2.7 mmol) in dichloromethane (200 mL), and sodium hydroxide (10.78 g, 269 mmol) in water (20 mL) at 0 °C over a period of 5 min. The resulting mixture was stirred at 0 °C for 1 h. The reaction mixture was diluted with dichloromethane (100 mL) and washed with water (2 × 100 mL). The organic layer was dried, filtered, and evaporated to afford crude product, which was triturated with methanol to give a solid that was collected by filtration and dried under vacuum to give **4** (23.8 g, 78%) as a beige powder. ^{1}H NMR δ 7.53 (1H, dd), 7.61−7.69 (2H, m), 7.72−7.79 (1H, m), 8.12−8.18 (2H, m), 8.44 (1H, s), 8.51 (1H, d), 9.28 (1H, d); *m*/*z* (ES+) $(M + H)^+$ = 339; HPLC t_R = 2.38 min.

1-(Phenylsulfonyl)-3-(4,4,5,5-tetramethyl-1,3,2-dioxaborolan-2-yl)-1*H*-pyrrolo[2,3-*c*]pyridine (5). $PdCl_2$(dppf) (1.3 g, 1.8 mmol) was added in one portion to 4,4,4′,4′,5,5,5′,5′-octamethyl-2,2′-bi(1,3,2-dioxaborolane) (5.4 g, 21 mmol), compound **4** (6 g, 17.8 mmol), and potassium acetate (5.9 g, 60.5 mmol) in dimethoxyethane (170 mL) at 25 °C under nitrogen. The resulting mixture was stirred at 80 °C for 18 h. The reaction mixture was evaporated to dryness and dissolved in ethyl acetate (600 mL), water was added (500 mL), and the mixture was shaken and filtered through dicalite. The ethyl acetate layer was separated and washed with saturated brine (500 mL). The organic layer was dried and filtered. This was poured onto a plug of silica and eluted with ethyl acetate (1.5 L) to give a pink solid, which was triturated with diethyl ether to afford **5** (5.2 g, 76%) as a white solid. ^{1}H NMR δ 1.33 (12H, s), 7.65 (2H, t), 7.73−7.80 (2H, m), 8.18−8.25 (3H, m), 8.43 (1H, d), 9.24 (1H, d); *m*/*z* (ESI+) $(M + H)^+$ = 303; HPLC t_R = 0.83 min.

3-(2-Chloropyrimidin-4-yl)-1-(phenylsulfonyl)-1*H*-pyrrolo-[2,3-*c*]pyridine (6). Tetrakis(triphenylphosphine)palladium(0) (0.78 g, 0.7 mmol) was added in one portion to 2,4-dichloropyrimidine (3 g, 20 mmol), compound **5** (5.2 g, 13.5 mmol), and 2 M sodium carbonate (27 mL, 54 mmol) in dioxane (80 mL) at 25 °C under nitrogen. The resulting mixture was stirred at 80 °C for 1 h. The reaction mixture was allowed to cool and then quenched with water (750 mL), and the precipitate was collected by filtration, washed with water, and dried under vacuum to afford crude product as a green solid. This was preadsorbed onto silica and purified by flash silica chromatography (elution gradient 0−100% ethyl acetate in isohexane). Pure fractions were evaporated to dryness to afford **6** (1.33 g, 27%) as a yellow solid. ^{1}H NMR δ 7.64−7.71 (2H, m), 7.75−7.81 (1H, m), 8.19−8.26 (2H, m), 8.29 (1H, d), 8.39 (1H, dd), 8.57 (1H, d), 8.82 (1H, d), 9.23 (1H, s), 9.32 (1H, d); *m*/*z* (ES+) $(M + H)^+$ = 371; HPLC t_R = 2.35 min.

3-(2-Chloropyrimidin-4-yl)-1*H*-pyrrolo[2,3-*c*]pyridine (7). Compound **6** (1.26 g, 3.4 mmol) and 2 M aqueous sodium carbonate (8.5 mL, 17 mmol) were suspended in dioxane (80 mL) and sealed into a microwave tube. The reaction was heated at 120 °C for 30 min in the microwave reactor and cooled to room temperature. The mixture was diluted with water (80 mL), and the organic solvent was removed by rotary evaporation. This gave a solid that was collected by filtration and dried under vacuum to give **7** (0.8 g, 100%) as a yellow

DOI: 10.1021/acs.jmedchem.5b00098
J. Med. Chem. XXXX, XXX, XXX−XXX

solid. ^{1}H NMR δ 7.97 (1H, d), 8.29 (1H, dd), 8.33 (1H, d), 8.61 (1H, d), 8.70 (1H, s), 12.53 (1H, brs); m/z (ES+) $(M + H)^+$ = 231; HPLC t_R = 2.16 min.

3-(2-Chloropyrimidin-4-yl)-1-methyl-1*H*-pyrrolo[2,3-*c*]-pyridine (8). Sodium hydride (151 mg, 3.8 mmol) was added in one portion to compound **7** (790 mg, 3.4 mmol) in DMF (20 mL) at 0 °C under nitrogen. The resulting mixture was stirred at 0 °C for 30 min, and then iodomethane (0.22 mL, 3.6 mmol) was added dropwise. The mixture was stirred and allowed to warm to ambient temperature over 2 h. The reaction mixture was diluted with ethyl acetate (100 mL) and washed sequentially with water (3 × 100 mL) and saturated brine (100 mL). The organic layer was dried, filtered, and evaporated to afford crude product, which was purified by flash silica chromatography (elution gradient 0−5% 7 M ammonia/methanol in dichloromethane). Pure fractions were evaporated to dryness to afford **8** (146 mg, 17%) as a yellow solid. ^{1}H NMR δ 4.02 (3H, s), 7.88 (1H, d), 8.27 (1H, dd), 8.38 (1H, d), 8.62 (1H, d), 8.68 (1H, s), 8.98 (1H, d); m/z (ES+) $(M + H)^+$ = 245; HPLC t_R = 2.29 min.

***N*-(2-Methoxy-4-(4-methylpiperazin-1-yl)phenyl)-4-(1-methyl-1*H*-pyrrolo[2,3-*c*]pyridin-3-yl)pyrimidin-2-amine (19).** 2-Methoxy-4-(4-methylpiperazin-1-yl)aniline (132 mg, 0.6 mmol), compound **8** (73 mg, 0.3 mmol) and 4-methylbenzenesulfonic acid hydrate (170 mg, 0.9 mmol) were dissolved in NMP (3 mL) and sealed into a microwave tube. The reaction was heated at 200 °C for 2 h and cooled. The reaction mixture was diluted with water, and saturated sodium bicarbonate was added. This was extracted with ethyl acetate, and the combined organic extracts were washed with water and saturated brine. The organic layer was dried, filtered, and evaporated to afford crude product, which was purified by flash silica chromatography (elution gradient 0−6% 7 N ammonia/methanol in dichloromethane). Pure fractions were evaporated to dryness to afford **19** (30 mg, 23%) as a solid. ^{1}H NMR δ 2.26 (3H, s), 2.48−2.54 (4H, m), 3.17 (4H, t), 3.81 (3H, s), 3.98 (3H, s), 6.56 (1H, dd), 6.68 (1H, d), 7.12 (1H, d), 7.71 (1H, d), 7.95 (1H, s), 8.18−8.25 (2H, m), 8.28 (1H, d), 8.44 (1H, s), 8.90 (1H, s); HRMS: ESI$^+$ m/z calcd, 430.2277; found, 430.23438 $(M + H)^+$; HPLC t_R = 2.86 min.

(*E*)-3-(2-Styrylpyrimidin-4-yl)-1*H*-pyrrolo[2,3-*c*]pyridine (31). Tetrahydrofuran (2.15 mL) was added in one portion to *trans*-beta-styreneboronic acid (0.048 g, 0.32 mmol), compound **6** (0.1 g, 0.27 mmol), $PdCl_2(PPh_3)_2$ (9.5 mg, 0.01 mmol), and *tri*-potassium phosphate trihydrate (0.11 g, 0.54 mmol) at 25 °C and sealed into a microwave tube. The reaction was heated at 130 °C for 30 min in the microwave reactor and cooled. 2 N sodium carbonate (600 μL) was added to the reaction and sealed into a microwave tube. The reaction was heated at 140 °C for 1 h and cooled. The reaction was evaporated to dryness, and DMF (3 mL) was added, the mixture was filtered, and the filtrate was purified by preparative HPLC using decreasingly polar mixtures of water (containing 1% ammonia) and acetonitrile as eluents. Fractions containing the desired compound were evaporated to dryness, and the material was further purified by ion exchange chromatography, using a 1g SCX-3 column. The desired product was eluted from the column using 7 M ammonia in methanol, and pure fractions were evaporated to dryness to afford **31** (0.03 g, 39%) as a solid. ^{1}H NMR δ 7.41 (1H, d), 7.42−7.55 (3H, m), 7.81−7.88 (3H, m), 8.09 (1H, d), 8.39 (1H, d), 8.58 (1H, dd), 8.70 (1H, s), 8.74 (1H, d), 8.92 (1H, d), 12.38 (1H, s); HRMS: ESI$^+$ m/z calcd, 298.1218; found, 299.12888 $(M + H)^+$; HPLC t_R = 2.13 min.

1-(1*H*-Pyrrolo[2,3-*c*]pyridin-3-yl)ethanone (9). Aluminum chloride (16.9 g, 127 mmol) was added in one portion to 1*H*-pyrrolo[2,3-*c*]pyridine **2** (3 g, 25.39 mmol) in DCM (596 mL) at 25 °C under nitrogen. The resulting mixture was stirred at 25 °C for 1 h. To this was added acetyl chloride (9 mL, 127 mmol) dropwise over 15 min. The reaction mixture was stirred at 25 °C for 18 h under nitrogen. The reaction mixture was quenched with methanol (80 mL) dropwise (cautious) with cooling in a water bath. The reaction mixture was evaporated to dryness, dissolved in water, and purified by ion exchange chromatography, using an SCX-2 column, washing the column well with water and then MeOH. The desired product was eluted from the column using 7 M ammonia in methanol, and pure fractions were evaporated to dryness to afford **9** (3 g, 74%) as a yellow solid. ^{1}H NMR δ 2.49 (3H, s), 8.05 (1H, dd), 8.28 (1H, d), 8.49 (1H, s), 8.83 (1H, d), 12.32 (1H, s); m/z (ES+) $(M + H)^+$ = 160.79, HPLC t_R = 1.39 min.

1-(1-(Phenylsulfonyl)-1*H*-pyrrolo[2,3-*c*]pyridin-3-yl)-ethanone (10). Benzenesulfonyl chloride (5.1 mL, 40 mmol) was added dropwise to compound **9** (5.3 g, 33 mmol), tetrabutylammonium hydrogensulfate (0.34 g, 1 mmol), sodium hydroxide (4 g, 100 mmol) in dichloromethane (100 mL), and water (20 mL) cooled to 0 °C over a period of 5 min. The resulting suspension was stirred at 0 °C for 40 min. The layers were separated, and the aqueous layer was extratced with dichloromethane (100 mL). The combined organic layers were then washed with water (100 mL) and concentrated to dryness. The crude residue was triturated with methanol to give a solid, which was collected by filtration and dried under vacuum to give **10** (5.8 g, 58%) as a white solid. ^{1}H NMR δ 2.61 (3H, s), 7.68 (2H, dt), 7.75−7.82 (1H, m), 8.10 (1H, dd), 8.25 (2H, dt), 8.49 (1H, d), 9.00 (1H, s), 9.25 (1H, d); m/z (ES+) $(M + H)^+$ = 301.09; HPLC t_R = 2.49 min.

(*E*)-3-(Dimethylamino)-1-(1-(phenylsulfonyl)-1*H*-pyrrolo[2,3-*c*]pyridin-3-yl)prop-2-en-1-one (11). 1,1-Di-*tert*-butoxy-*N*,*N*-dimethylmethanamine (0.4 mL, 1.7 mmol) was added in one portion to compound **10** (100 mg, 0.33 mmol) in DMF (2 mL). The resulting solution was stirred at 80 °C for 2.5 h. The mixture was then concentrated to dryness and triturated with ether to give a dark green solid, which was purified by flash silica chromatography)elution gradient 0−10% methanol in dichloromethane). Pure fractions were evaporated to dryness to afford **11** (76 mg, 64%) as a yellow solid. ^{1}H NMR δ 2.98 (3H, s), 3.15 (3H, s), 5.96 (1H, d), 7.61−7.72 (3H, m), 7.77 (1H, t), 8.12−8.19 (2H, m), 8.22 (1H, dd), 8.43 (1H, d), 8.85 (1H, s), 9.23 (1H, d); m/z (ES+) $(M + H)^+$ = 356.37; HPLC t_R = 1.85 min.

3-(2-Methylpyrimidin-4-yl)-1*H*-pyrrolo[2,3-*c*]pyridine (32). Compound **11** (0.5 g, 1.4 mmol), acetimidamide hydrochloride (0.67 g, 7 mmol), and potassium 2-methylpropan-2-olate (0.95 g, 8.4 mmol) were suspended in DMA (20 mL) and sealed into a microwave tube. The reaction was heated at 150 °C for 1 h in the microwave reactor and cooled. The reaction mixture was filtered through Celite and concentrated to dryness. The crude product was purified by flash silica chromatography (elution gradient 0−10% 7 M ammonia/methanol in DCM). Pure fractions were evaporated to dryness to afford **32** (0.22 g, 73%) as a cream solid. ^{1}H NMR δ 3.29 (3H, s), 7.72 (1H, d), 8.27 (1H, d), 8.40 (1H, dd), 8.54−8.58 (2H, m), 8.83 (1H, d), 12.26 (1H, br s); HRMS: ESI$^+$ m/z calcd, 211.0905; found, 211.09802 $(M + H)^+$; HPLC t_R = 1.86 min.

1-Benzyl-3-(2-methylpyrimidin-4-yl)-1*H*-pyrrolo[2,3-*c*]-pyridine (33). Tri-*n*-butylphosphine (0.24 mL, 0.95 mmol) was added in one portion to compound **32** (100 mg, 0.5 mmol), benzyl alcohol (0.1 mL, 0.95 mmol), and (*E*)-diisopropyl diazene-1,2-dicarboxylate (0.19 mL, 0.95 mmol) in degassed THF (4 mL) under nitrogen. The resulting solution was stirred for 18 h and then diluted with methanol, and the crude product was was purified by preparative HPLC using decreasingly polar mixtures of water (containing 1% ammonia) and acetonitrile as eluents. Fractions containing the desired compound were evaporated to dryness to afford **33** (55 mg, 39%) as a white solid. ^{1}H NMR δ 2.66 (3H, s), 5.63 (2H, s), 7.24−7.40 (5H, m), 7.69 (1H, d), 8.30 (1H, d), 8.38 (1H, dd), 8.59 (1H, d), 8.75 (1H, s), 8.95 (1H, d); HRMS: ESI$^+$ m/z calcd, 301.1374; found, 301.14432 $(M + H)^+$; HPLC t_R = 1.06 min.

■ ASSOCIATED CONTENT

Supporting Information

Protocols for the enzyme and cell assays, synthetic methods for the remaining examples, crystallographic information, and kinase panel selectivity data for compounds in Table 5. This material is available free of charge via the Internet at http://pubs.acs.org.

DOI: 10.1021/acs.jmedchem.5b00098
J. Med. Chem. XXXX, XXX, XXX−XXX

AUTHOR INFORMATION

Corresponding Author

*Tel.: +441625 517920. E-mail: jason.kettle@astrazeneca.com.

Present Address

[†](M.C.) Cancer Research UK Manchester Institute, University of Manchester, Wilmslow Road, Manchester M20 4BX, United Kingdom.

Notes

The authors declare no competing financial interest.

REFERENCES

(1) (a) Lee, K.-M.; Deng, X.; Friedman, E. Mirk protein kinase is a mitogen-activated protein kinase substrate that mediates survival of colon cancer cells. *Cancer Res.* **2000**, *60*, 3631−3637. (b) Mercer, S. E.; Ewton, D. Z.; Deng, X.; Lim, S.; Mazur, T. R.; Friedman, E. Myrk/Dyrk1B mediates survival during the differentiation of C2C12 myoblasts. *J. Biol. Chem.* **2005**, *280*, 25788−25801.

(2) Becker, W.; Joost, H. G. Structural and functional characteristics of Dyrk, a novel subfamily of protein kinases with dual specificity. *Prog. Nucleic Acid Res. Mol. Biol.* **1999**, *62*, 1−17.

(3) Friedman, E. Mirk/Dyrk1B in cancer. *J. Cell. Biochem.* **2007**, *102*, 274−279.

(4) Hu, J.; Deng, H.; Friedman, E. A. Ovarian cancer cells, not normal cells, are damaged by Mirk/Dyrk1B kinase inhibition. *Int. J. Cancer* **2013**, *132*, 2258−2269.

(5) Yang, C.; Ji, D.; Weinstein, E. J.; Choy, E.; Hornicek, F. J.; Wood, K. B.; Liu, X.; Mankin, H.; Duan, Z. The kinase Mirk is a potential therapeutic target in osteosarcoma. *Carcinogenesis* **2010**, *31*, 552−558.

(6) Keramati, A. R.; Fathzadeh, M.; Go, G.-W.; Singh, R.; Choi, M.; Faramarzi, S.; Mane, S.; Kasaei, M.; Sarajzadeh-Fard, K.; Hwa, J.; Kidd, K. K.; Babaee Bigi, M. A.; Malekzadeh, R.; Hosseinian, A.; Babaei, M.; Lifton, R. P.; Mani, A. A form of the metabolic syndrome associated with mutations in DYRK1B. *N. Engl. J. Med.* **2014**, *370*, 1909−1919.

(7) (a) Loidreau, Y.; Marchand, P.; Dubouilh-Benard, C.; Nourrisson, M.-R.; Duflos, M.; Loaëc, N.; Meijer, L.; Besson, T. Synthesis and biological evaluation of *N*-aryl-7-methoxybenzo[*b*]furo-[3,2-*d*]pyrimidin-4-amines and their *N*-arylbenzo[*b*]thieno[3,2-*d*]-pyrimidin-4-amine analogues as dual inhibitors of CLK1 and DYRK1A kinases. *Eur. J. Med. Chem.* **2013**, *59*, 283−295. (b) Wang, D.; Wang, F.; Tan, Y.; Dong, L.; Chen, L.; Zhu, W.; Wang, H. Discovery of potent small molecule inhibitors of DYRK1A by structure-based virtual screening and bioassay. *Bioorg. Med. Chem. Lett.* **2012**, *22*, 168−171.

(8) Altafaj, X.; Dierssen, M.; Baamonde, C.; Marti, E.; Visa, J.; Guimera, J.; Oset, M.; Gonzalex, J.; Florez, J.; Fillat, C.; Estivill, X. Neurodevelopmental delay, motor abnormalities and cognitive defects in transgenic mice overexpressing Dyrk1A (minibrain), a murine model of Down's syndrome. *Hum. Mol. Genet.* **2001**, *10*, 1915−1923.

(9) Metro, G.; Chiari, R.; Baldi, A.; De Angelis, V.; Minotti, V.; Crino, L. Selumetinib: a promising pharmacologic approach for KRAS-mutant advanced non-small-cell lung cancer. *Future Oncol.* **2013**, *9*, 167−177.

(10) Cohen, R. B.; Aamdal, S.; Nyakas, M.; Cavallin, M.; Green, D.; Learoyd, M.; Smith, I.; Kurzrock, R. A phase I dose-finding, safety and tolerability study of AZD8330 in patients with advanced malignancies. *Eur. J. Cancer* **2013**, *49*, 1521−1529.

(11) (a) Anderson, K.; Chen, Y.; Chen, Z.; Dominique, R.; Glenn, K.; He, Y.; Janson, C.; Luk, K.-C.; Lukacs, C.; Polonskaia, A.; Qiao, Q.; Railkar, A.; Rossman, P.; Sun, H.; Xiang, Q.; Vilenchik, M.; Wovkulich, P.; Zhang, X. Pyrido[2,3-d]pyrimidines: discovery and preliminary SAR of a novel series of DYRK1B and DYRK1A inhibitors. *Bioorg. Med. Chem. Lett.* **2013**, *23*, 6610−6615. (b) Coombs, T. C.; Tanega, C.; Shen, M.; Wang, J. L.; Auld, D. S.; Gerritz, S. W.; Schoenen, F. J.; Thomas, C. J.; Aube, J. Small-molecule pyrimidine inhibitors of the cdc2-like (Clk) and dual specificity tyrosine phosphorylation-regulated (Dyrk) kinases: development of chemical probe ML315. *Bioorg. Med. Chem. Lett.* **2013**, *23*, 3654−3661. (c) Rosse, G. Tricyclic pyrimidines as inhibitors of DYRK1A/DYRK1B as potential treatment for Down's syndrome or Alzheimer's disease. *ACS Med. Chem. Lett.* **2013**, *4*, 502−503. (d) Schmitt, C.; Kail, D.; Mariano, M.; Empting, M.; Weber, N.; Paul, T.; Hartmann, R. W.; Engel, M. Design and synthesis of a library of lead-like 2,4-bisheterocyclic substituted thiophenes as selective Dyrk/Clk inhibitors. *PLoS One* **2014**, *9*, e87851.

(12) Göckler, N.; Jofre, G.; Papadopoulos, C.; Soppa, U.; Tejedor, F. J.; Becker, W. Harmine specifically inhibits protein kinase Dyrk1A and interferes with neurite formation. *FEBS J.* **2009**, *276*, 6324−6337.

(13) Bain, J.; Palter, L.; Elliott, M.; Shpiro, N.; Hastie, C. J.; McLauchlan, H.; Klevernic, I.; Arthur, J. S.; Alessi, D. R.; Cohen, P. The selectivity of protein kinase inhibitors: a further update. *Biochem. J.* **2007**, *408*, 297−315.

(14) Song, Y.; Kesuma, D.; Wang, J.; Deng, Y.; Duan, J.; Wang, J. H.; Qi, R. Z. Specific inhibition of cyclin-dependent kinases and cell proliferation by harmine. *Biochem. Biophys. Res. Commun.* **2004**, *317*, 128−132.

(15) Waki, H.; Park, K. W.; Mitro, N.; Pei, L.; Damoiseaux, R.; Wilpitz, D. C.; Reue, K.; Saez, E.; Tontonoz, P. The small molecule harmine is an antidiabetic cell-type-specific regulator of PPARgamma expression. *Cell Metab.* **2007**, *5*, 357−370.

(16) Kim, H.; Sablin, S. O.; Ramsay, R. R. Inhibition of monoamine oxidase A by beta-carboline derivatives. *Arch. Biochem. Biophys.* **1997**, *337*, 137−142.

(17) Ducray, R.; Simpson, I.; Jung, F. H.; Nissink, J. W. M.; Kenny, P. W.; Fitzek, M.; Walker, G. E.; Ward, L. T.; Hudson, K. Discovery of novel imidazo[1,2-*a*]pyridines as inhibitors of the insulin-like growth factor-1 receptor tyrosine kinase. *Bioorg. Med. Chem. Lett.* **2011**, *21*, 4698−4701.

(18) Kothe, M.; Kohls, D.; Low, S.; Coli, R.; Rennie, G. R.; Feru, F.; Kuhn, C.; Ding, Y.-H. Selectivity-determining residues in Plk1. *Chem. Biol. Drug Des.* **2007**, *70*, 540−546.

(19) Anderson, D. R.; Meyers, M. J.; Vernier, W. F.; Mahoney, M. W.; Kurumbail, R. G.; Caspers, N.; Poda, G. I.; Schindler, J. F.; Reitz, D. B.; Mourey, R. J. Pyrrolopyridine inhibitors of mitogen-activated protein kinase-activated protein kinase 2 (MK-2). *J. Med. Chem.* **2007**, *50*, 2647−2654.

(20) Wrobleski, S. T.; Lin, S.; Dhar, T. G.; Dyckman, A. J.; Li, T.; Pitt, S.; Zhang, R.; Fan, Y.; Doweyko, A. M.; Tokarski, J. S.; Kish, K. F.; Kiefer, S. E.; Sack, J. S.; Newitt, J. A.; Witmer, M. R.; McKinnon, M.; Barrish, J. C.; Dodd, J. H.; Schieven, G. L.; Leftheris, K. The identification of novel p38α isoform selective kinase inhibitors having an unprecedented p38α binding mode. *Bioorg. Med. Chem. Lett.* **2013**, *23*, 4120−4126.

(21) Medina, J. R. Selective 3-phosphoinositide-dependent kinase 1 (PDK1) inhibitors: dissecting the function and pharmacology of PDK1. *J. Med. Chem.* **2013**, *56*, 2726−2737.

(22) Ashford, A. L.; Oxley, D.; Kettle, J.; Hudson, K.; Guichard, S.; Cook, S. J.; Lochhead, P. A. A novel DYRK1B inhibitor AZ191 demonstrates that DYRK1B acts independently of GSK3β to phosphorylate cyclin D1 at Thr286, not Thr288. *Biochem. J.* **2014**, *457*, 43−56.

DOI: 10.1021/acs.jmedchem.5b00098
J. Med. Chem. XXXX, XXX, XXX−XXX